Rotationally resolved photoelectron spectra in resonance enhanced multiphoton ionization of H2O via the C 1 B 1 Rydberg state

M.-T. Lee, Kwanghsi Wang, V. McKoy, and L. E. Machado

Citation: The Journal of Chemical Physics **97**, 3905 (1992); doi: 10.1063/1.462929
View online: http://dx.doi.org/10.1063/1.462929
View Table of Contents: http://scitation.aip.org/content/aip/journal/jcp/97/6?ver=pdfcov
Published by the AIP Publishing

Rotationally resolved photoelectron spectra in resonance enhanced multiphoton ionization of H_2O via the $C\ ^1B_1$ Rydberg state

M.-T. Lee,[a] Kwanghsi Wang, and V. McKoy
Arthur Amos Noyes Laboratory of Chemical Physics,[b] California Institute of Technology, Pasadena, California 91125

L. E. Machado
Departamento de Fisica, Universidade Federal de São Carlos, Caixa Postal 676, 13560 São Paulo, Brazil

(Received 27 April 1992; accepted 3 June 1992)

In this paper, we extend a previous formulation of molecular resonance enhanced multiphoton ionization (REMPI) photoelectron spectra of diatomic molecules to treat rotationally resolved photoionization of nonlinear polyatomic molecules. Useful parity selection rules, which govern changes of angular momenta ΔK_a and ΔK_c, are also derived. As an example, we use this formulation to study rotational branching ratios and photoelectron angular distributions resulting from (3+1′) REMPI of H_2O via the $C\ ^1B_1$ ($3pa_1$) Rydberg state. Cooper minima are predicted to occur in the d wave ($l=2$) of the ka_1 ($\lambda=0$) and kb_1 ($\lambda=1$) photoelectron continua. The effects of these Cooper minima on rotationally resolved photoelectron spectra are also investigated.

I. INTRODUCTION

Resonance enhanced multiphoton ionization coupled with high-resolution photoelectron spectroscopy (REMPI-PES) provides a useful probe of molecular excited states and the photoionization dynamics of these states.[1,2] In REMPI, a single rotational level of the resonant state is selected and therefore only a small number of rotational levels of the ion are generally accessed. This results in substantial simplification in the photoelectron spectra, making such spectra particularly useful in investigating the photoionization dynamics of nonlinear molecules.[3] Such rotationally resolved ion spectra of nonlinear molecules (NH_3, C_6H_6, IHI, *para*-difluorobenzene, phenol-H_2O, and pyrazine) have been studied by zero-kinetic-energy (ZEKE) photoelectron spectroscopy.[3] For ZEKE detection, the spectral resolution is about the laser bandwidth ($\sim 0.1\ cm^{-1}$) which readily provides for rotational resolution in molecular ions.

We have previously given a formulation[4–6] for REMPI photoelectron spectra of diatomic molecules which explicitly used multiplet-specific final-state wave functions for the photoionized system. With the aid of parity selection rules such as $\Delta N+l=$odd,[5–8] ($\Delta N = N_+ - N_i$, where N_+ and N_i are the rotational quantum numbers of the ionic and intermediate states, respectively, and l is an angular momentum component of the photoelectron), we have exploited this formulation to quantitatively account for ion rotational distributions and the effects of Cooper minima on such distributions resulting from REMPI of Rydberg states of diatomic molecules (NO, CH, H_2, and OH).[4,5,9–11] Here this formulation is extended to characterize rotationally resolved REMPI spectra of nonlinear molecules. In this paper, emphasis is placed on molecules of C_{2v} symmetry. Useful formulas and associated parity selection rules are obtained. This formulation has been used recently to interpret successfully the dynamical origins of type a transitions seen in the experiments of Tonkyn *et al.*[12,13] in photoionization of jet-cooled water with coherent vacuum ultraviolet (VUV) radiation.

Our formulation is used here to study REMPI spectra resulting from (3+1′) REMPI of the $C\ ^1B_1$ Rydberg state of H_2O. We choose this specific example for the following reasons: Recently, Kuge and Kleinermanns[14] have studied the rotational predissociation of H_2O by (3+1) REMPI of the $C\ ^1B_1$ ($3pa_1$) Rydberg state in a supersonic jet. However, the REMPI ion spectra for ionization of a specific rotational level of the resonant $C\ ^1B_1$ state were not rotationally resolved and, hence, the associated photoionization dynamics and ion rotational propensity rules were not transparent. Meanwhile, Tonkyn *et al.*[12] have investigated the rotationally resolved single-photon VUV ZEKE photoelectron spectra of jet-cooled water by pulsed field ionization of extremely high-n Rydberg states. Both type a and type c transitions were observed in these ion spectra in contrast to the prediction of type c transitions only by Child and Jungen.[15] Lee *et al.*[13] have accounted successfully for these type a transitions as arising from nonatomic-like behavior of the molecular photoelectron continua. Of particular interest here is to examine related behavior which may be also associated with REMPI spectra of the $C\ ^1B_1$ Rydberg state of H_2O.

Results of theoretical studies of ion rotational distributions and associated photoelectron angular distributions are presented here for (3+1′) REMPI via the $C\ ^1B_1$ ($3pa_1$) Rydberg state of H_2O. Examination of angular momentum components of photoelectron matrix elements reveal that Cooper minima[10,11,16–21] are associated with these photoionization continua. Cooper minima have been shown previously to have pronounced effects on ion rotational distributions. For example, they give rise to an un-

[a] Permanent address: Departamento de Química, Universidade Federal de São Carlos, Caixa Posta 676, CEP 13560 São Paulo, Brazil.
[b] Contribution No. 8620.

expected $\Delta N=0$ peak in REMPI spectra of the $D\,^2\Sigma^+(3p\sigma)$ Rydberg state of NO,[10] the $D\,^2\Sigma^-(3p\sigma)$ state of OH,[11] and the $f\,^1\Pi(3p\sigma)$ state of NH.[20,21] These effects of Cooper minima on rotationally resolved photoelectron spectra of nonlinear molecules are also studied here at various kinetic energies. To our knowledge, Cooper minima in the photoionization of excited states of nonlinear molecules have not been reported previously.

II. THEORY AND NUMERICAL DETAILS

A. Rotationally resolved ($n+1'$) REMPI theory

($n+1'$) REMPI processes via a resonant intermediate state of any molecule can be viewed as a two-step process of n-photon absorption from an unaligned initial (or ground) state (all M_{J_0} sublevels are equally populated) to the resonant intermediate state, followed by subsequent one-photon ionization of the aligned intermediate state. The photon energies of the excitation and ionization steps of REMPI may differ from each other in a two-color experiment. Under collision-free conditions, each M_J channel can be treated as an independent ionization channel for linearly polarized light. The differential cross section for photoionization of the resonant state by the final photon can then be written as

$$\frac{d\sigma}{d\Omega} \propto \sum_{M_{J_i}M_{J_+}} \rho_{M_{J_i}M_{J_i}} |\Gamma_{M_{J_i}M_{J_+}}|^2$$

$$= \frac{\sigma}{4\pi}\left[1+\sum_{L=1}\beta_{2L}P_{2L}(\cos\theta)\right], \tag{1}$$

where σ is the total cross section, β_{2L} is an asymmetry parameter, $P_{2L}(\cos\theta)$ is a Legendre polynominal, $|\Gamma_{M_{J_i}M_{J_+}}|^2$ is the ionization probability out of the M_{J_i} magnetic sublevel of the intermediate state leading to the M_{J_+} sublevel of the ion, $\rho_{M_{J_i}M_{J_i}}$ is the population of the M_{J_i} sublevel induced by the n-photon excitation, and J_i and J_+ are the total angular momenta of the intermediate and ionic states in the laboratory frame, respectively. Note that subscripts i and $+$ denote the quantum numbers for the intermediate and ionic states, respectively. The evaluation of $\rho_{M_{J_i}M_{J_i}}$ usually requires a summation over all dipole-allowed virtual states and possible paths. However, in many cases, explicit evaluation of these summations is not necessary if one is interested only in the relative population (the alignment) of the different M_{J_i} sublevels of the intermediate state. Under these circumstances, $\rho_{M_{J_i}M_{J_i}}$ has the simple form

$$\rho_{M_{J_i}M_{J_i}} = \begin{pmatrix} J_i & n & J_0 \\ -M_{J_i} & 0 & M_{J_i}\end{pmatrix}^2 B \tag{2}$$

with B the rotational line strength (which is just an overall multiplicative factor) and J_0 the rotational quantum number of the initial state.

We now examine the matrix element for photoionization of an M_{J_i} sublevel of the resonant state leading to an M_{J_+} sublevel of the final continuum state. The following formulation is generally derived for asymmetric top molecules. However, the application of this formulation to a symmetric top is straightforward. The bound–free transition moment $\Gamma_{M_{J_i}M_{J_+}}$ can be written as

$$\Gamma_{M_{J_i}M_{J_+}} = \sum_{\Lambda_f\Sigma_f} \langle\phi_e|\langle f^+|\Lambda_f\Sigma_f\rangle\langle\Lambda_f\Sigma_f|D_{\mu_0}|i\rangle, \tag{3}$$

where

$$D_{\mu_0} = \sqrt{\frac{4\pi}{3}}\, r \sum_{\mu} (-1)^{\mu_0-\mu}\mathscr{D}^1_{\mu_0\mu}Y_{1\mu}(\hat{r}) \tag{4}$$

with D_{μ_0} the dipole moment operator in the laboratory frame and $\mathscr{D}^1_{\mu_0\mu}$ rotational matrices in Edmonds' notation.[22] In Eq. (3), the total final-state continuum wave function (ion+photoelectron)

$$|f\rangle = \sum_{\Lambda_f\Sigma_f} |\Lambda_f\Sigma_f\rangle\langle\Lambda_f\Sigma_f|f\rangle \tag{5}$$

is used where $|\Lambda_f\Sigma_f\rangle$ is a dipole-allowed multiplet-specific final-state wave function.

To evaluate $\Gamma_{M_{J_i}M_{J_+}}$, explicit forms for wave functions of the intermediate state $|i\rangle$, ionic state $|f^+\rangle$, and photoelectron $|\phi_e\rangle$ are necessary. They have the forms

$$|i\rangle = \psi_i\chi_{v_i}(-1)^{N_i-S_i+M_{J_i}}(2J_i+1)^{1/2}\begin{pmatrix} N_i & S_i & J_i \\ M_{N_i} & M_{S_i} & -M_{J_i}\end{pmatrix} \times |S_iM_{S_i}\rangle|N_iM_{N_i}K_{a_i}K_{c_i}\rangle, \tag{6}$$

$$|f^+\rangle = \psi_+\chi_{v_+}(-1)^{N_+-S_++M_{J_+}}(2J_++1)^{1/2} \times \begin{pmatrix} N_+ & S_+ & J_+ \\ M_{N_+} & M_{S_+} & -M_{J_+}\end{pmatrix} \times |S_+M_{S_+}\rangle|N_+M_{N_+}K_{a_+}K_{c_+}\rangle, \tag{7}$$

and

$$|\phi_e\rangle = \left(\frac{2}{\pi}\right)^{1/2}\left|\frac{1}{2}m_\sigma\right\rangle \sum_{\gamma q h l\lambda}\frac{i^l}{k}\phi^{(-)\gamma q}_{hl\lambda}(\mathbf{r})X^{*\gamma q}_{hl\lambda}(\hat{k}), \tag{8}$$

where $|\frac{1}{2}m_\sigma\rangle$ is the spin eigenfunction of the photoelectron, k defines the photoelectron kinetic energy, γ is one of the irreducible representations (IR) of the molecular point group, q is a component of this representation, h distinguishes between different bases for the same IR corresponding to the same value of l, $\phi^{(-)\gamma q}_{hl\lambda}(\mathbf{r})$ is a partial wave component of the photoelectron orbital, $X^{\gamma q}_{hl\lambda}(\hat{\mathbf{k}})$ is a generalized harmonic, and ψ_i and χ_{v_i} are the electronic and vibrational wave functions of the state $|i\rangle$, respectively. Note that Hund's case (b) coupling scheme is chosen to represent both the intermediate and ionic states [see Eqs. (6) and (7)]. The rotational levels of both intermediate and ionic states are described by the asymmetric top wave function

$$|NM_NK_aK_c\rangle = \sum_K a_{N\tau K}S(NM_NKp), \tag{9}$$

where $\tau = K_a - K_c$ with K_a and K_c the projections of the total angular momentum along the a and c axes, respectively, and the coefficients $a_{N\tau K}$ are determined by diagonalizing the rigid rotor Hamiltonian

$$H_r=\frac{J_x^2}{2I_x}+\frac{J_y^2}{2I_y}+\frac{J_z^2}{2I_z} \tag{10}$$

in the basis of the symmetric top eigenfunctions. In Eq. (9), $S(NM_NKp)$ is a linear combination of symmetric top functions and has the form[23]

$$S(NM_NKp)=\frac{1}{\sqrt{2}}\left[|NM_NK\rangle+(-1)^p|NM_N-K\rangle\right] \tag{11}$$

for $K>0$ with p the parity index having the value of 0 or 1, and

$$S(NM_N00)=|NM_N0\rangle \tag{12}$$

for $K=0$. The symmetric top wave functions $|NM_NK\rangle$ in Eqs. (11) and (12) are given by

$$|NM_NK\rangle=\left(\frac{2N+1}{8\pi^2}\right)^{1/2}(-1)^{K-M_N}\mathscr{D}^N_{M_NK}. \tag{13}$$

Note that the $S(NM_NKp)$ functions adopted in Eq. (9) instead of symmetric top eigenfunctions $|NM_NK\rangle$ fulfill the symmetry requirements of the V_4 group.[23] In Eq. (8), we use the generalized harmonics $X^{\gamma q}_{hl\lambda}(\hat{k})$ as bases for the IR of the molecular point group. These symmetry-adapted angular functions satisfy well-known orthonormality relations[24] and can be expressed in terms of the usual spherical harmonics

$$X^{\gamma q}_{hl\lambda}(\hat{k})=b^{\gamma q}_{hl\lambda}Y_{l\lambda}(\hat{k})+b^{\gamma q}_{hl-\lambda}Y_{l-\lambda}(\hat{k}) \tag{14}$$

in the body-fixed frame. The coefficients $b^{\gamma q}_{hl\lambda}$ for the C_{2v} and O_h symmetries have been given by Burke *et al.*[24] These $Y_{l\lambda}(\hat{k})$ can be further written in terms of the spherical harmonics $Y_{lm}(\hat{k}')$ in the laboratory frame as

$$Y_{l\lambda}(\hat{k})=\sum_m(-1)^{\lambda-m}\mathscr{D}^l_{m\lambda}Y_{lm}(\hat{k}'). \tag{15}$$

By substituting Eqs. (4) and (6)–(8) into Eq. (3) and making use of the properties of 3-j symbols, Eq. (3) can be rewritten as

$$\Gamma_{M_{J_i}M_{J_+}}=\sum_{lm}C_{lm}(M_{J_i}M_{J_+})Y_{lm}(\hat{k}'), \tag{16}$$

where

$$\begin{aligned}C_{lm}(M_{J_i}M_{J_+})=&\sqrt{\frac{4\pi}{3}}\frac{1}{2}\left[(2J_i+1)(2J_++1)(2N_i+1)(2N_++1)(2S_i+1)\right]^{1/2}\sum(-1)^Q(2N_t+1)\\
&\times\begin{pmatrix}S_+ & \frac{1}{2} & S_i\\ M_{S_+} & m_\sigma & -M_{S_i}\end{pmatrix}\begin{pmatrix}N_+ & S_+ & J_+\\ M_{N_+} & M_{S_+} & -M_{J_+}\end{pmatrix}\begin{pmatrix}N_i & S_i & J_i\\ M_{N_i} & M_{S_i} & -M_{J_i}\end{pmatrix}\begin{pmatrix}N_+ & N_i & N_t\\ -M_{N_+} & M_{N_i} & m_t\end{pmatrix}\\
&\times\begin{pmatrix}N_t & 1 & l\\ -m_t & \mu_0 & m\end{pmatrix}\times a_{N_i\tau_iK_i}a_{N_+\tau_+K_+}\tilde{I}^{\gamma q}_{hl\lambda\mu}(\Lambda_f\Sigma_f)b^{\gamma q}_{hl\lambda}(\Lambda_f\Sigma_f)\left[1+(-1)^{\Delta p+\Delta N+l+1}\right]\\
&\times\left[\begin{pmatrix}N_+ & N_i & N_t\\ -K_+ & K_i & K_t\end{pmatrix}\begin{pmatrix}N_t & 1 & l\\ -K_t & \mu & \lambda\end{pmatrix}+(-1)^{p_+}\begin{pmatrix}N_+ & N_i & N_t\\ K_+ & K_i & K_t\end{pmatrix}\begin{pmatrix}N_t & 1 & l\\ -K_t & \mu & \lambda\end{pmatrix}\right],\end{aligned} \tag{17}$$

$$Q=\Delta N+\Delta M_J-S_i+M_{S_i}-\mu_0-m+M_{N_+}+K_i-1/2, \tag{18}$$

$$\begin{aligned}\tilde{I}^{\gamma q}_{hl\lambda\mu}(\Lambda_f\Sigma_f)=&\langle\gamma_+q_+\gamma_eq_e|\Lambda_f\rangle\\
&\times\langle M_{S_+}m_\sigma|\Sigma_f\rangle I^{\gamma q}_{hl\lambda\mu}(\Lambda_f\Sigma_f),\end{aligned} \tag{19}$$

and

$$\begin{aligned}I^{\gamma q}_{hl\lambda\mu}(\Lambda_f\Sigma_f)=&\sqrt{\frac{2}{\pi}}\frac{(-i)^l}{k}\int dR\,dr\,\psi^*_+(\mathbf{r},R)\chi^*_{v_+}(R)\\
&\times\phi^{*(-)\gamma q}_{hl\lambda}(\mathbf{r},R)rY_{1\mu}\psi_i(\mathbf{r},R)\chi_{v_i}(R),\end{aligned} \tag{20}$$

with $\Delta p=p_+-p_i$, $\Delta M_J=M_{J_+}-M_{J_i}$, and the summation in Eq. (17) goes over all possible indices. Substituting Eq. (16) into Eq. (1), it is easy to verify that

$$\sigma\propto\sum_{\substack{lm\\M_{J_i}M_{J_+}}}\rho_{M_{J_i}M_{J_i}}|C_{lm}(M_{J_i}M_{J_+})|^2 \tag{21}$$

and

$$\begin{aligned}\beta_{2L}=&\frac{4L+1}{\sigma}\sum_{\substack{ll'm\\M_{J_i}M_{J_+}}}(-1)^m(2l+1)(2l'+1)\\
&\times\rho_{M_{J_i}M_{J_i}}C_{lm}(M_{J_i}M_{J_+})C^*_{l'm}(M_{J_i}M_{J_+})\\
&\times\begin{pmatrix}l & l' & 2L\\ m & -m & 0\end{pmatrix}\begin{pmatrix}l & l' & 2L\\ 0 & 0 & 0\end{pmatrix}.\end{aligned} \tag{22}$$

Furthermore, for the branching ratios of interest here, the constant implied in Eqs. (1) and (21) is unimportant and

will be suppressed. Equations (21) and (22) are also suitable for photoionization of symmetric top molecules except that $a_{N\tau K}$ of Eq. (17) becomes unity for both the intermediate and ionic states.

B. Parity selection rule

Equation (17) yields the general parity selection rule

$$\Delta N+\Delta p+l=\text{odd}, \tag{23}$$

which has the same form as for diatomic molecules for Hund's case (b) coupling.[5–8] However, this selection rule is not particularly transparent since the parity indices p_i and p_+ are defined with respect to the $S(NM_NKp)$ functions used to expand the asymmetric top wave functions [see Eq. (11)]. Equation (23) should be modified to reveal explicitly its dependence on the angular momentum changes ΔK_a and ΔK_c.

Here we choose a left-handed coordinate system for the molecular internal x, y, and z axes with the molecular z axis as the symmetry axis. With the symmetry properties of the asymmetric top,[23] it can be shown that ΔK_η is even (odd) when $\Delta N+\Delta p$ is even (odd), where η is the principal axis lying along the molecular x axis and K_η is the projection of the total angular momentum along this axis. The parity selection rule of Eq. (23) then reduces to

$$\Delta K_\eta+l=\text{odd}. \tag{24}$$

The selection rules also depend on which principal axis coincides with the molecular z axis. With the properties of 3-j symbols, Eq. (17) provides additional selection rules[23]

$$\mu+\lambda=\begin{cases}\Delta K_a, & \text{if } a//z// \text{ the symmetry axis}\\ \Delta K_b, & \text{if } b//z// \text{ the symmetry axis}\\ \Delta K_c, & \text{if } c//z// \text{ the symmetry axis}\end{cases}. \tag{25}$$

To relate the selection rules of Eqs. (24) and (25), a relationship among ΔK_a, ΔK_b, and ΔK_c is essential. This relationship, which can be obtained from the symmetry properties of asymmetric top,[23] is

$$\Delta K_a+\Delta K_c=\text{even (odd)}\leftrightarrow\Delta K_b=\text{even (odd)}. \tag{26}$$

For example, if the molecular axes x, y, and z coincide with the b, c, and a axes, respectively, the selection rules of Eqs. (24) and (25) become $\Delta K_b + l =$ odd and $\mu + \lambda = \Delta K_a$, respectively. Determination of $\mu+\lambda$ now becomes a critical step in the application of these selection rules. Whereas Eqs. (24)–(26) are suitable for any nonlinear polyatomic molecule, $\mu+\lambda$ must be determined specifically for a given molecular symmetry.

To illustrate these selection rules, (3+1′) REMPI via the $C\,^1B_1$ ($3pa_1$) Rydberg state of H_2O is taken as an example. The molecular x, y, and z axes are chosen to coincide with the a, c, and b axes, respectively, for H_2O and H_2O^+. Therefore, the selection rules of Eqs. (24) and (25) become

$$\Delta K_a+l=\text{odd} \tag{27}$$

and

$$\mu+\lambda=\Delta K_b, \tag{28}$$

respectively. For the C_{2v} symmetry of H_2O and H_2O^+, the x, y, and z components of the dipole moment operator belong to the b_2, b_1, and a_1 irreducible representations, respectively. There are three corresponding dipole-allowed continuum channels kb_2, kb_1, and ka_1 for photoionization from the $3pa_1$ orbital of the $C\,^1B_1$ Rydberg state leading to the $X\,^2B_1$ ground state of the ion. In this case, odd λ and μ are associated with the kb_1 and kb_2 channels, whereas even λ and μ are associated with the ka_1 channel. Therefore $\lambda+\mu$ is always even for all allowed transitions. Thus, from Eq. (28), we have $\Delta K_b =$ even. Based on the relationship of Eq. (26), we have

$$\Delta K_a+\Delta K_c=\text{even}. \tag{29}$$

Equations (27) and (29) show that only type b transitions are allowed. These transitions with $\Delta K_a =$ odd and $\Delta K_c =$ odd are associated with even l partial waves of the photoelectron matrix elements and those of $\Delta K_a =$ even and $\Delta K_c =$ even with odd l partial waves. However, type a ($\Delta K_a =$ even and $\Delta K_c =$ odd) and type c ($\Delta K_a =$ odd and $\Delta K_c =$ even) transitions are forbidden.

C. (3+1′) REMPI via the $C\,^1B_1$ Rydberg state of H_2O

There are three dipole-allowed transition channels for photoionization of the $3pa_1$ orbital of the $C\,^1B_1$ Rydberg state. The corresponding multiplet-specific final-state wave functions $|\Lambda_f\Sigma_f\rangle$ of Eq. (5) are given by

$$\Psi(^1B_1)=\frac{1}{\sqrt{2}}\left[|(\text{core})1b_1\overline{ka_1}|-|(\text{core})\overline{1b_1}ka_1|\right], \tag{30a}$$

$$\Psi(^1A_1)=\frac{1}{\sqrt{2}}\left[|(\text{core})1b_1\overline{kb_1}|-|(\text{core})\overline{1b_1}kb_1|\right], \tag{30b}$$

and

$$\Psi(^1A_2)=\frac{1}{\sqrt{2}}\left[|(\text{core})1b_1\overline{kb_2}|-|(\text{core})\overline{1b_1}kb_2|\right], \tag{30c}$$

where $(\text{core})=1a_1^2 2a_1^2 3a_1^2 1b_2^2$. Within the frozen-core Hartree–Fock model for the final state, the photoelectron orbital ϕ_k can be shown to be a solution of the one-electron Schrödinger equation of the form[25,26]

$$P\left(f+\sum_{i=\text{core}}(2J_i-K_i)+a_nJ_n+b_nK_n-\epsilon\right)P|\phi_k\rangle=0, \tag{31}$$

where J_i and K_i are the Coulomb and exchange operators, respectively, and P is a projection operator which enforces orthogonality of the continuum orbital to the occupied orbitals.[25,26] The photoelectron kinetic energy is given by $\epsilon = \frac{1}{2}k^2$. The one-electron operator f in Eq. (31) is

$$f=-\tfrac{1}{2}\nabla_i^2-\sum_\alpha\frac{Z_\alpha}{\mathbf{r}_{i\alpha}}, \tag{32}$$

where Z_α is a nuclear charge. Using the wave functions of Eq. (30), the coefficients a_n and b_n associated with $1b_1$ orbital assume the value of 1.

For the wave function of the $C\,^1B_1(1b_1 \rightarrow 3pa_1)$ resonant state, we use the improved virtual orbital (IVO) method[27] in which the core orbitals are taken to be those of the fully relaxed $^2B_1$ ion. The orbital basis used in these calculations consists of a $(6s4p)$ contraction of the $(10s6p)$ primitive Cartesian Gaussian functions of Dunning[28] augmented by three s ($\alpha=0.065$, 0.016, and 0.004), three p ($\alpha=0.065$, 0.012, and 0.003), and four d ($\alpha=1.322$, 0.3916, 0.09, and 0.02) functions on the oxygen atom. On the hydrogen, we use a $(3s)$ contraction of the $(4s)$ primitive Cartesian Gaussian functions of Dunning[28] augmented by three s ($\alpha=0.072$, 0.018, and 0.0045) and four p ($\alpha=1.12$, 0.1296, 0.03, and 0.006) functions. With this basis and choice of wave functions, we obtain a total energy of $-75.745\,462$ a.u. for the $C\,^1B_1$ Rydberg state at the known equilibrium geometry ($R_{O\text{-}H}=1.8085$ a.u. and $\theta_{H\text{-}O\text{-}H}=104.5°$).[29] The single-center expansion of the $3pa_1$ orbital around the center of mass shows 12.97% s, 77.96% p, 8.65% d, and 0.41% f character, respectively.

To obtain the photoelectron orbital ϕ_k, we have used an iterative procedure, based on the Schwinger variational principle,[25,26] to solve the Lippmann–Schwinger equation associated with Eq. (31). This procedure begins by approximating the static-exchange potential of the relaxed ionic core by a separable form

$$U(\mathbf{r},\mathbf{r}')=\sum_{ij}\langle\mathbf{r}|U|\alpha_i\rangle(U^{-1})_{ij}\langle\alpha_i|U|\mathbf{r}'\rangle, \qquad (33)$$

where the matrix U^{-1} is the inverse of the matrix with the elements $(U)_{ij}=\langle\alpha_i|U|\alpha_j\rangle$ and the α's are discrete basis functions such as Cartesian or spherical Gaussian functions. U is twice the static-exchange potential in Eq. (31) with the long-term Coulomb potential removed. The Lippmann–Schwinger equation with this separable potential $U(\mathbf{r},\mathbf{r}')$ can be readily solved and provides an approximate photoelectron orbital $\phi_k^{(0)}$. These $\phi_k^{(0)}$ can be iteratively improved to yield converged solutions to the Lippmann–Schwinger equation containing the full static-exchange potential. In this study, four iterations provided converged solutions of Eq. (31). The scattering basis sets used in the separable expansion of Eq. (33) are listed in Table I.

All matrix elements arising in the solution of the Lippmann–Schwinger equation and elsewhere were evaluated by using single-center expansions about the center of mass. For converged results, the maximum partial wave used in the expansions of bound orbitals, potentials, and photoelectron continuum orbital was seven. For the electron nuclear potential, 14 partial waves were used. Runs with larger partial wave expansions showed that our calculated cross sections are converged. The radial integration grid extended to 73 a.u. and contained 600 points. The integration step sizes ranged from 0.005 to 0.16 up to 9 a.u. and up to 0.32 a.u. beyond this point.

TABLE I. Basis sets used in the separable potential of Eq. (33).

Symmetry	Center	Cartesian Gaussian function[a]	Exponents (α)
a_1	O	s	16.0, 8.0, 4.0, 2.0, 1.0, 0.5, 0.25, 0.1
		z	4.0, 2.0, 1.0, 0.5, 0.1
		x^2	1.0, 0.5, 0.1
		y^2	1.0, 0.5, 0.1
		z^2	1.0, 0.5, 0.1
	H	s	2.0, 1.0, 0.5, 0.1
		x	0.5, 0.1
b_1	O	y	4.0, 2.0, 1.0, 0.5, 0.1
		yz	1.0, 0.1
	H	y	1.0, 0.5, 0.1
b_2	O	x	8.0, 4.0, 2.0, 1.0, 0.5, 0.1
		xz	2.0, 1.0, 0.5, 0.1
	H	s	2.0, 1.0, 0.5, 0.1
		x	2.0, 1.0, 0.5, 0.1

[a]Defined as $\phi^{\alpha,l,m,n,\mathbf{A}}(\mathbf{r}) = \mathcal{N}(x-A_x)^l(y-A_y)^m(z-A_z)^n \exp(-\alpha|\mathbf{r}-\mathbf{A}|^2)$ with $\mathcal{N}$ a normalization constant.

III. RESULTS AND DISCUSSION

In Fig. 1, we show the total cross sections and the asymmetry parameter β as a function of photon energy for photoionization of the $C\,^1B_1$ $(3pa_1)$ Rydberg state of H_2O leading to the $X\,^2B_1$ ionic ground state. The partial cross sections associated with the $3pa_1 \rightarrow ka_1$, $3pa_1 \rightarrow kb_1$, and $3pa_1 \rightarrow kb_2$ channels are also shown in Fig. 1(a). The total cross section and partial cross sections of the ka_1 and kb_1 channels decrease sharply near threshold. A minimum

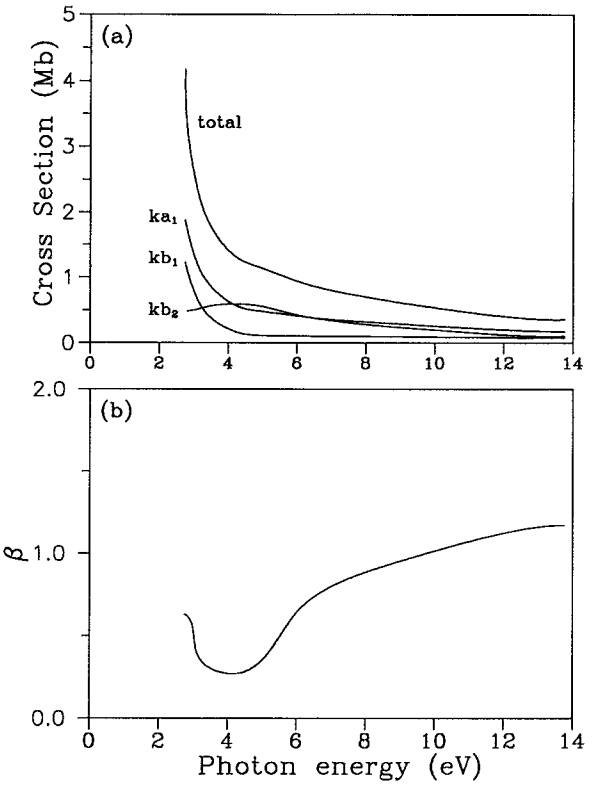

FIG. 1. Cross sections and asymmetry parameters β for photoionization of the $3pa_1$ orbital of the $C\,^1B_1$ Rydberg state of H_2O leading to the $X\,^2B_1$ ground state of H_2O^+. An ionization potential of 2.61 eV is assumed. Partial cross sections associated with the ka_1, kb_1, and kb_2 ionization channels are also shown.

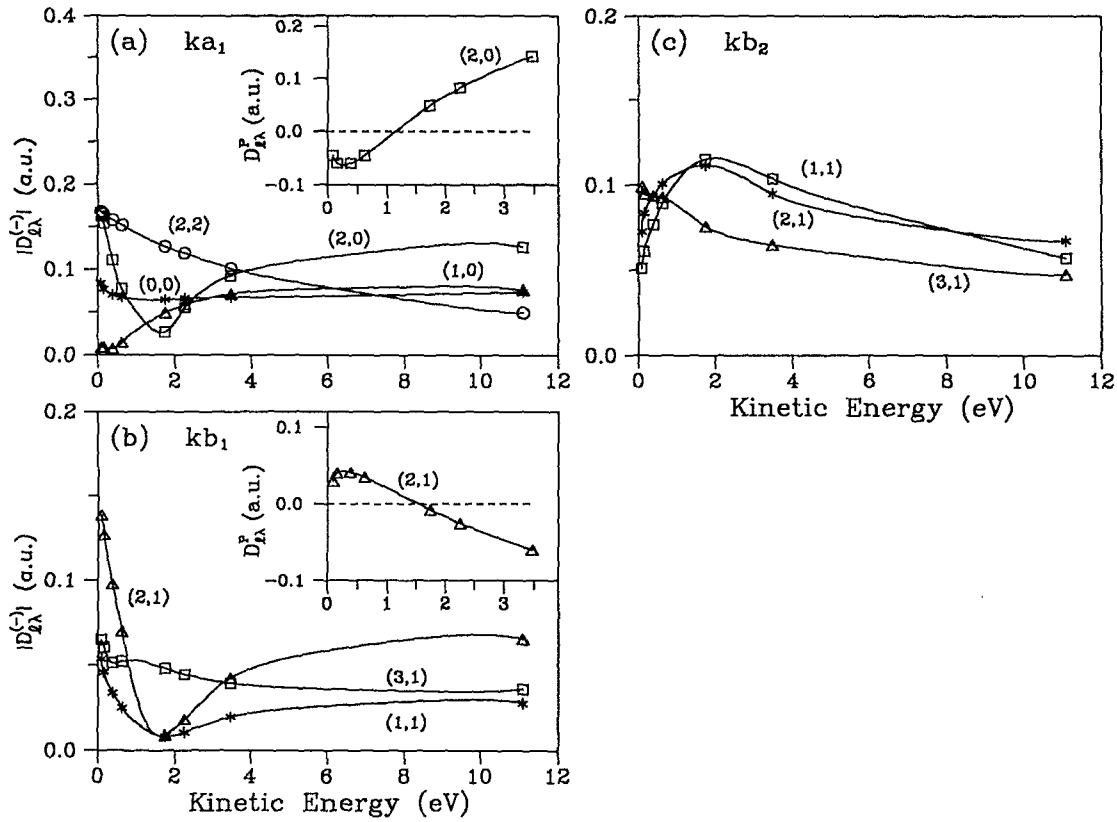

FIG. 2. Magnitude $|D^{(-)}_{l\lambda}|$ of the partial wave photoionization matrix elements as a function of kinetic energy for the (a) $3pa_1 \rightarrow ka_1$; (b) $3pa_1 \rightarrow kb_1$; and (c) $3pa_1 \rightarrow kb_2$ channels for the $C\,^1B_1$ Rydberg state. (l,λ) denotes each component of $|D^{(-)}_{l\lambda}|$. The insets show the principal-value dipole amplitude $D^{P}_{l\lambda}$ for the $l=2$ component.

is clearly seen in the asymmetry parameter [Fig. 1(b)] around 4 eV. To identify the physical origin of this minimum, Fig. 2 shows the magnitude $|D^{(-)}_{l\lambda}|$ of the incoming-wave normalized partial wave dipole amplitude as a function of kinetic energy for the $3pa_1 \rightarrow ka_1$ [Fig. 2(a)], $3pa_1 \rightarrow kb_1$ [Fig. 2(b)], and $3pa_1 \rightarrow kb_2$ [Fig. 2(c)] channels for several important partial wave components. For each channel, $D^{(-)}_{l\lambda}$ represents one component of μ in $I^{qq}_{h\lambda\mu}$ [Eq. (20)]. Note that in C_{2v} symmetry, q and h indices are not required since the representations are all one dimensional. Note also that (l,λ) is used to label components of $|D^{(-)}_{l\lambda}|$ in Fig. 2. Minima are seen clearly in the (2,0) component of the ka_1 channel and (2,1) component of the kb_1 channel. Examining the principal-value dipole amplitude $D^{P}_{l\lambda}$ (standing-wave normalized) shown in the insets of Figs. 2(a) and 2(b), a sign change is seen in the d wave of the $ka_1(\lambda = 0)$ and $kb_1(\lambda = 1)$ channels. This indicates the presence of Cooper minima which are responsible for the minimum in the asymmetry parameter β of Fig. 1(b). No minimum is seen in the cross sections [Fig. 1(a)], since other components such as (2,2) in the ka_1 channel and the (3,1) component in the kb_1 channel are predominant in the vicinity of Cooper minima in $|D^{(-)}_{l\lambda}|$. These Cooper minima are essentially similar to those found in photoionization of atoms,[16,17] ground state of molecules,[18] and Rydberg state of diatomic molecules,[10,11,19–21] except that these minima also depend on λ. Cooper minima have been shown to have pronounced effects on photoelectron spectra for photoionization of Rydberg states of diatomic molecules.[19–21] It is clearly of interest to see what role these λ-dependent Cooper minima may play in the rotationally resolved photoionization dynamics.

Figure 3 shows the calculated ion rotational distributions resulting from (3+1) REMPI via the 3_{12} [Fig. 3(a)] and 3_{30} [Fig. 3(b)] rotational levels of the $C\,^1B_1$ Rydberg state. Here the rotational level is denoted by $N_{K_aK_c}$. Both rotational levels originate from the 0_{00} rotational level of *para* water via three-photon excitation, i.e., the $T(0)$ rotational branch. Since the rotational line strength B of Eq. (2) is just an overall constant here, the alignment of the 3_{12} and 3_{30} rotational levels can be determined individually from the 3-j symbols of Eq. (2). The photoelectron kinetic energy is about 0.72 eV. The calculated spectra are convoluted with a Gaussian detection function having a full width at half-maximum (FWHM) of 1.5 meV. Dominant rotational levels in the ion spectra are labeled. Note that both rotational levels of the $C\,^1B_1$ state have the same N quantum number and alignment $\rho_{M_{J_i}M_{J_i}}$. Interesting features of these ion rotational distributions include: (*i*) strong ΔK_a = odd and ΔK_c = odd transitions expected on the basis of the dominant (even) partial-wave components of the photoelectron matrix element, arising from the p character of the $3pa_1$ orbital of the $C\,^1B_1$ state; (*ii*) strong

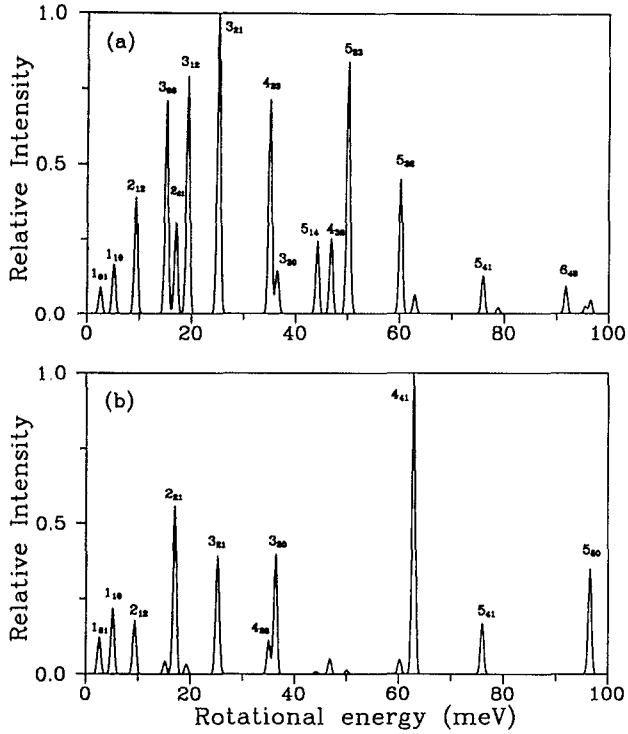

FIG. 3. Calculated ionic rotational branching ratios resulting from (3 +1) REMPI via the (a) 3_{12} and (b) 3_{30} rotational levels of the $C\,^1B_1$ Rydberg state. The photoelectron kinetic energy is about 0.72 eV. Each transition is convoluted with a Gaussian detection function with a FWHM of 1.5 meV. The highest intensity has been normalized to unity.

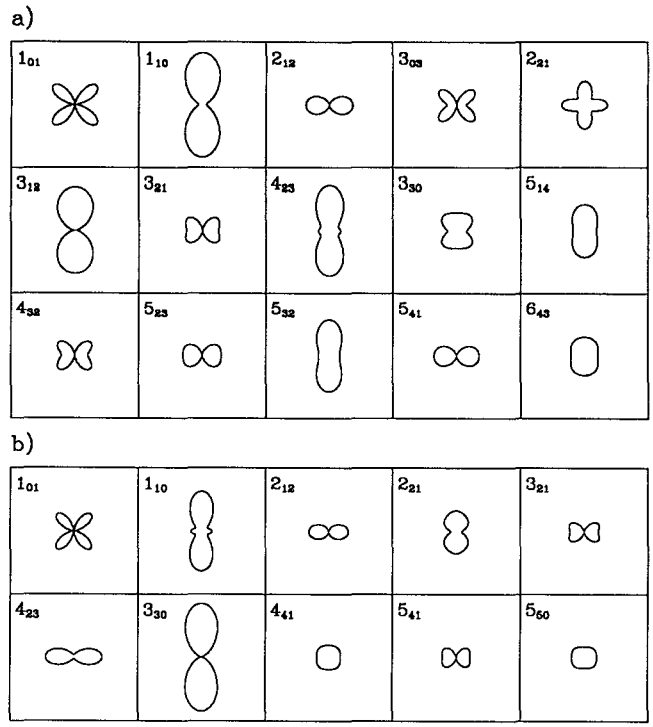

FIG. 4. Calculated photoelectron angular distributions for the rotational levels of Fig. 3. The polarization direction is vertical (θ=0°).

K_a and K_c dependencies of the ion rotational branching ratios [cf. Figs. 3(a) and 3(b)], since ΔK_a, ΔK_c, and ΔN depend on angular momentum component l of the photoelectron; (iii) the same $\Delta K_a = 1$ and $|\Delta K_c| = 1$ angular momentum changes for the most intense transitions via the different rotational levels of the C state, even though ΔN angular momentum changes are different (ΔN=0 and 1 are associated with the most intense peak of the photoelectron spectra of the 3_{12} and 3_{30} rotational levels, respectively); (iv) strong ΔN=0, ±1, and ±2 transitions satisfying the requirements, of angular momentum transfer N_t {i.e., $|l-1| \leqslant N_t \leqslant l+1$ and $N_t \geqslant |\Delta N|$ [see Eq. (17)]} and (v) unexpected ΔK_a = even and ΔK_c = even transitions which would arise from odd partial wave contributions to the photoelectron matrix element. At the equilibrium geometry, the $3pa_1$ Rydberg orbital has about 20% even partial waves (s and d waves), and the $3s \rightarrow kp$, $3d \rightarrow kp$, and $3d \rightarrow kf$ transitions contribute substantially to the total transition moment. The l=3 (f wave) continuum is also important and contributes mainly to the $\Delta N = \pm 2$ (ΔK_a = even and ΔK_c = even) peaks. These transitions, which arise from odd angular momentum components of the photoelectron continuum, are comparable in intensity with those of even partial waves. For example, the $3_{12} \rightarrow 3_{12}$ transition (odd wave contributions) has almost the same intensity as the most intense $3_{12} \rightarrow 3_{21}$ transition which arises from even continuum waves [see Fig. 3(a)]. The presence of these *relatively* strong odd continuum waves reflects angular momentum coupling induced by the strongly anisotropic molecular ion potential. This behavior is similar to that responsible for type *a* transitions observed in the photoionization of ground state H_2O.[12,13]

To illustrate the angular momentum composition of these photoelectron continua, Fig. 4 shows the photoelectron angular distributions associated with the ion spectra of Fig. 3. Terms up to β_6 of Eq. (1) are included. In these plots, we assume β_0=1 and θ=0° is vertical. Evidence of higher partial wave contributions are seen clearly especially for transitions with $\Delta N = -2$. Interference between partial waves of the photoelectron matrix element and between different ionization channels is important since these angular distributions are admixtures of various angular momentum components. These photoelectron angular distributions reflect the angular composition of the photoelectron upon ionization. Also, according to the selection rules of Eqs. (27)–(29), transitions with ΔK_a = even and ΔK_c = even arise from odd partial waves and those with ΔK_a = odd and ΔK_c = odd from even continuum waves.

Figures 5 and 6 show the calculated ion rotational distributions and associated photoelectron angular distributions, respectively, for (3+1) REMPI via the (a) 4_{13} and (b) 4_{31} rotational levels of the $C\,^1B_1$ Rydberg state. Both rotational levels are populated by three-photon excitation from the ground rotational level 1_{01} of *ortho* water, i.e., the $T(1)$ rotational line. The calculated spectra are convoluted with a Gaussian detection function with a FWHM of 1.5 meV. Important features associated with photoionization of *para* water (Figs. 3 and 4) are also seen here except that the angular momentum changes (ΔN, ΔK_a, and ΔK_c) as-

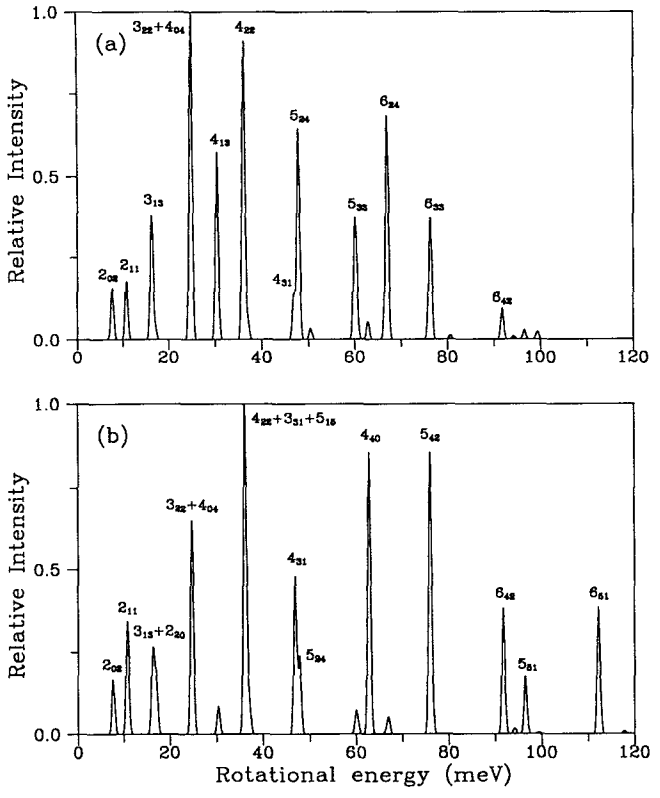

FIG. 5. The same as in Fig. 3 except for (3+1) REMPI via the (a) 4_{13} and (b) 4_{31} rotational levels of the C state.

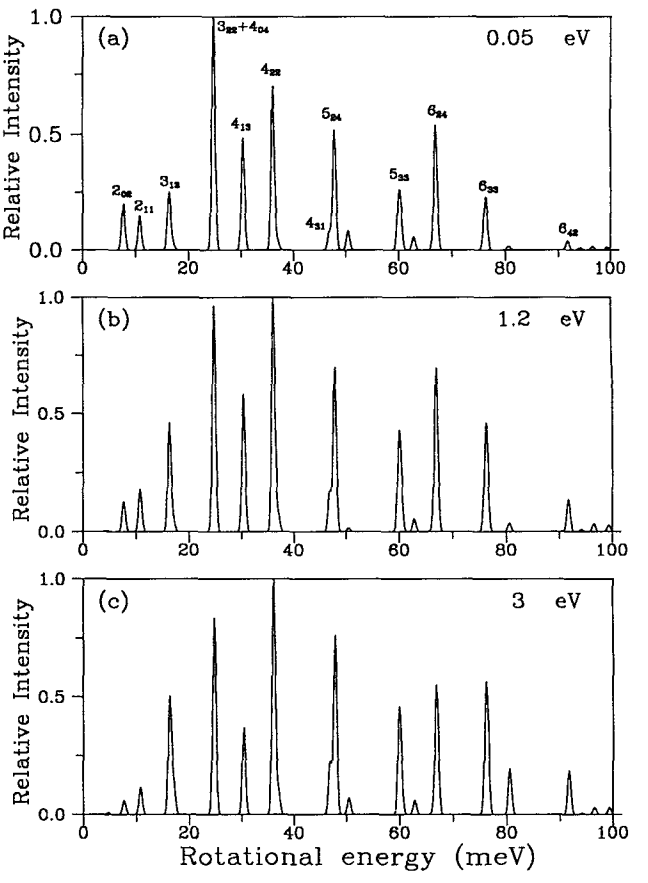

FIG. 7. Calculated ionic rotational branching ratios resulting from (3+1′) REMPI via the 4_{13} rotational level of the $C\,^1B_1$ Rydberg state at (a) 0.05; (b) 1.2; and (c) 3 eV of kinetic energies. The other notation is the same as in Fig. 3.

sociated with the most intense peaks of Figs. 3(a) ($3_{12}\rightarrow 3_{21}$) and 3(b) ($3_{30}\rightarrow 4_{41}$) and Figs. 5(a) ($4_{13}\rightarrow 3_{22}$) and 5(b) ($4_{31}\rightarrow 4_{22}$) are different. It is interesting to note that the difference between the spectral profiles of Figs. 5(a) and 5(b) arises from the changes of the values of K_a and K_c in the C state.

Unexpected ΔN=even (especially $\Delta N=0$) transitions have been observed in the ion spectra of NO, OH, and NH diatomic molecules in which Cooper minima play an important role.[10,11,20,21] These anomalous spectra arise primarily from the formation of Cooper minima in the $d(l=2)$ continuum wave. The depletion of the d wave contribution to the photoelectron matrix element in the vicinity of Cooper minima subsequently leads to an enhancement of the relative importance of the odd waves which make the dominant contributions to these unexpected $\Delta N=0$ transitions. Cooper minima are also predicted to occur here (see Fig. 2). However, Figs. 3 and 5 do not show as strong an influence of these Cooper minima on the ion distributions as was seen for diatomic molecules,[10,11,20,21] even though the photoelectron kinetic energies lie in the vicinity of these Cooper minima. The main reason is due to the significant contributions from other even wave components such as the (2,2) component in the ka_1 channel and (2,1) in the kb_2 channel. In Fig. 7, we show the photoelectron spectra for (3+1′) REMPI via the 4_{13} [$T(1)$ rotational branch] rotational level of the $C\,^1B_1$ Rydberg state at several kinetic energies. The range of kinetic energies is chosen to span both Cooper minima (see Fig. 2). The ion rotational branching ratios depend on photoelectron kinetic energy due to the changes in the (l,λ) partial wave composition of the matrix element $D_{l\lambda}^{(-)}$ around the Cooper minima. The effect of these Cooper minima are seen clearly from the photoelectron angular distributions shown in Fig. 8. Only

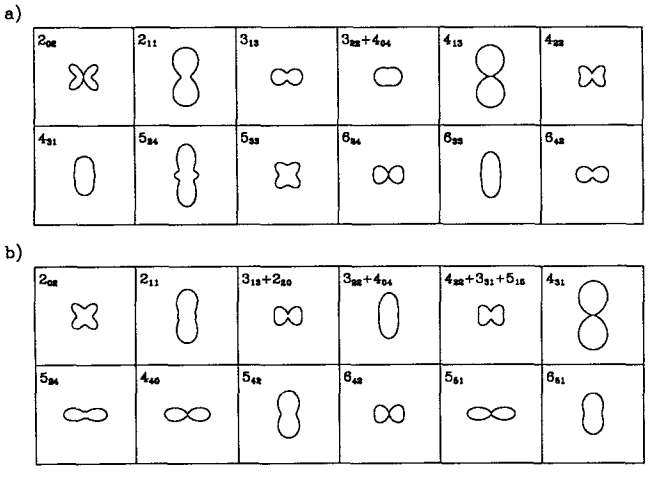

FIG. 6. Calculated photoelectron angular distributions for the rotational levels of Fig. 5. $\theta=0°$ is vertical.

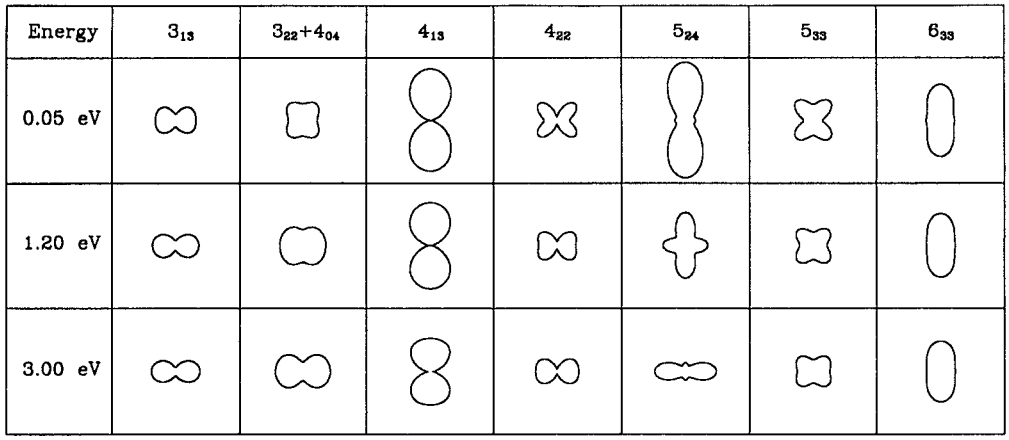

FIG. 8. Selected photoelectron angular distributions for the rotational levels of Fig. 7. $\theta=0°$ is vertical.

selected ionic rotational levels are shown. These Cooper minima at low kinetic energies may be particularly useful in exploring the ionization dynamics of excited states of H_2O.

ACKNOWLEDGMENTS

This work was supported by grants from the National Science Foundation, Air Force Office of Scientific Research, and the Office of Health and Environmental Research of the U.S. Department of Energy. We also acknowledge use of resources of the Jet Propulsion Laboratory/Caltech CRAY Y-MP2E/116 Supercomputer. One of us (M. T. L.) thanks the Conselho Nacional de Desenvolvimento Científico e Tecnológico (CNPq, Brazil) for financial support.

[1] R. N. Compton and J. C. Miller, in *Laser Applications in Physical Chemistry*, edited by D. K. Evans (Dekker, New York, 1988).
[2] S. T. Pratt, P. M. Dehmer, and J. L. Dehmer, in *Advances in Multiphoton Processes and Spectroscopy*, edited by S. H. Lin (World Scientific, Singapore, 1988), and the references and tabulation of REMPI-PES studies therein.
[3] K. Müller-Dethlefs and E. W. Schlag, Annu. Rev. Phys. Chem. **42**, 109 (1991), and references therein.
[4] S. N. Dixit, D. L. Lynch, V. McKoy, and W. M. Huo, Phys. Rev. A **32**, 1267 (1985).
[5] S. N. Dixit and V. McKoy, Chem. Phys. Lett. **128**, 49 (1986).
[6] K. Wang and V. McKoy, J. Chem. Phys. **95**, 4977 (1991).
[7] J. Xie and R. N. Zare, J. Chem. Phys. **93**, 3033 (1990).
[8] G. Raseev and N. Cherepkov, Phys. Rev. A **42**, 3948 (1990).
[9] H. Rudolph and V. McKoy, J. Chem. Phys. **91**, 2235 (1989); H. Rudolph, J. A. Stephens, V. McKoy, and M.-T. Lee, *ibid.* **91**, 1374 (1989).
[10] K. Wang, J. A. Stephens, and V. McKoy, J. Chem. Phys. **95**, 6456 (1991).
[11] E. de Beer, C. A. de Lange, J. A. Stephens, K. Wang, and V. McKoy, J. Chem. Phys. **95**, 714 (1991).
[12] R. G. Tonkyn, R. Wiedmann, E. R. Grant, and M. G. White, J. Chem. Phys. **95**, 7033 (1991).
[13] M.-T. Lee, K. Wang, V. McKoy, R. G. Tonkyn, R. Wiedmann, E. R. Grant, and M. G. White, J. Chem. Phys. **96**, 7848 (1992).
[14] H.-H. Kuge and K. Kleinermanns, J. Chem. Phys. **90**, 46 (1988).
[15] M. S. Child and Ch. Jungen, J. Chem. Phys. **93**, 7756 (1990).
[16] J. W. Cooper, Phys. Rev. **128**, 681 (1962); U. Fano and J. W. Cooper, Rev. Mod. Phys. **40**, 441 (1968); A. F. Starace, in *Handbuch der Physik*, edited by M. Mehlhorn (Springer, Berlin, 1982), Vol. 31, pp. 1–121.
[17] S. T. Manson, Phys. Rev. A **31**, 3698 (1985); A. Z. Msezane and S. T. Manson, Phys. Rev. Lett. **48**, 473 (1982).
[18] T. A. Carlson, M. O. Krause, W. A. Svensson, P. Gerard, F. A. Grimm, T. A. Whitley, and B. P. Pullen, Z. Phys. D **2**, 309 (1986).
[19] J. A. Stephens and V. McKoy, Phys. Rev. Lett. **62**, 889 (1989); J. Chem. Phys. **93**, 7863 (1990); K. Wang, J. A. Stephens, and V. McKoy, *ibid.* **93**, 7874 (1990); H. Rudolph and V. McKoy, *ibid.* **91**, 7995 (1989); **93**, 7054 (1990).
[20] E. de Beer, M. Born, C. A. de Lange, and N. P. C. Westwood, Chem. Phys. Lett. **186**, 40 (1991).
[21] K. Wang, J. A. Stephens, V. McKoy, E. de Beer, C. A. de Lange, and N. P. C. Westwood, J. Chem. Phys. **97**, 211 (1992).
[22] A. R. Edmonds, *Angular Momentum in Quantum Mechanics* (Princeton University, Princeton, N.J., 1974).
[23] R. S. Mulliken, Phys. Rev. **59**, 873 (1941).
[24] P. G. Burke, N. Chandra, and F. A. Gianturco, J. Phys. B **5**, 2212 (1972).
[25] R. R. Lucchese, G. Raseev, and V. McKoy, Phys. Rev. A **25**, 2572 (1982).
[26] R. R. Lucchese, K. Takatsuka, and V. McKoy, Phys. Rep. **131**, 147 (1986).
[27] W. J. Hunt and W. A. Goddard, Chem. Phys. Lett. **3**, 414 (1969).
[28] T. H. Dunning, Jr., J. Chem. Phys. **55**, 716 (1971).
[29] G. Herzberg, *Molecular Spectra and Molecular Structure III. Electronic Spectra and Electronic Structure of Polyatomic Molecules* (Van Nostrand, New York, 1966).